Advanced Membranes 7 (2026) 100193

Contents lists available at ScienceDirect

Advanced Membranes

journal homepage: www.keaipublishing.com/en/journals/advanced-membranes

Molecular fractionation with poly(ether ether ketone) hollow fibers

Banan Alhazmi[a,1], Lakshmeesha Upadhyaya[a,1], Shanshan Hong[b], Gergo Ignacz[c], Radosław Górecki[a], Maik Tepper[d,e], Hannah Roth[d,e], Matthias Wessling[d,e], Gyorgy Szekely[a,c], Suzana P. Nunes[a,b,c,*]

[a] Environmental Science and Engineering Program, Biological and Environmental Science and Engineering Division (BESE), King Abdullah University of Science and Technology (KAUST), Thuwal, Saudi Arabia
[b] Chemistry Program, Physical Science and Engineering Division (PSE), King Abdullah University of Science and Technology (KAUST), Thuwal, Saudi Arabia
[c] Chemical Engineering Program, Physical Science and Engineering Division (PSE), King Abdullah University of Science and Technology (KAUST), Thuwal, Saudi Arabia
[d] Chemical Process Engineering, RWTH Aachen University, Forckenbeckstrasse 51, 52074, Aachen, Germany
[e] DWI - Leibniz Institute for Interactive Materials, Forckenbeckstrasse 50, 52074, Aachen, Germany

ARTICLE INFO

Keywords:
PEEK
Hollow fibers
Membranes
3D printing
Organic solvent nanofiltration
API separation

ABSTRACT

Sustainable and efficient separation technologies are essential for minimizing the environmental impact of the chemical and pharmaceutical industries. Membranes with stability in solvents and precise molecular separation are needed. We report poly(ether ether ketone) (PEEK) membranes engineered for the separation of multi-component mixtures of active pharmaceutical ingredients (API) of different size and polarity. PEEK is highly stable in solvents typically used in the industry even without crosslinking, but the insolubility is a challenge for solution processing and fibers fabrication. We spun PEEK fibers from solutions in methanesulfonic acid through acid-resistant spinnerets designed and fabricated by stereolithography 3D printing, which are not susceptible to corrosion. Membranes with acetonitrile permeance of around 3 L m^{-2} h^{-1} bar^{-1} and over 90 % rejection of molecules with 120 g mol^{-1} were obtained. We also innovate in providing a comprehensive performance characterization that predicts the efficiency in separating molecule pairs of different size and chemistry, a procedure more representative of industrial applications instead of the commonly used screening with dye molecules, which can be prone to adsorption artefacts. We discuss the transport mechanisms of organic solvents through the membranes providing a comprehensive analysis of experimental results to evaluate the contributions of pore flow, permeant-polymer affinity and friction to the transport.

1. Introduction

Sustainable chemical and pharmaceutical industries require more competitive processes. Purifying, concentrating, and fractionating complex mixtures of active pharmaceutical ingredients (API) often involve energy-intensive multi-step processes with high solvent consumption. Organic solvent nanofiltration (OSN) has been introduced in the pharmaceutical industry, offering energy efficiency, cost savings, and a reduced environmental footprint [1–5]. The availability of highly selective solvent-resistant membranes with characteristics adequate to each process is primordial. Among the challenges are (1) the selection of stable polymer materials that are processible into membranes through typical solution-based methods like nonsolvent induced phase separation; (2) optimization of the fabrication method; and (3) characterization under conditions that would be representative of the target application.

In this work, to address the membrane materials and fabrication, we chose poly(ether ether ketone) (PEEK), which is one of the few polymeric materials that can be used in harsh solvent separations without crosslinking [6,7]. However, its solubility is restricted to a few solvents like sulfuric acid and methanesulfonic acid, which has mainly limited the industrial fabrication to processes based on melt extrusion [8–11]. Much less applied is nonsolvent-induced phase separation [12–17]. We recently introduced spinnerets designed and fabricated by stereolithography 3D

* Corresponding author. Environmental Science and Engineering Program, Biological and Environmental Science and Engineering Division (BESE), King Abdullah University of Science and Technology (KAUST), Thuwal, Saudi Arabia.
E-mail address: suzana.nunes@kaust.edu.sa (S.P. Nunes).
Peer review under the responsibility of Nanjing Tech University.
[1] Equal contribution as first authors.

https://doi.org/10.1016/j.advmem.2025.100193
Received 10 October 2025; Received in revised form 23 November 2025; Accepted 24 November 2025
Available online 27 November 2025
2772-8234/© 2025 The Authors. Publishing services by Elsevier B.V. on behalf of KeAi Communications Co. Ltd. This is an open access article under the CC BY-NC-ND license (http://creativecommons.org/licenses/by-nc-nd/4.0/).

printing of UV-curable rigid resins [18] for membrane fabrication and reported preliminary results with poly(ether ketone ketone) (PEKK) in sulfuric acid. Advantages are the more flexible design of the spinneret and the possibility of potentially corrosive dope solutions without concern. We applied now 3D printed spinnerets to prepare PEEK hollow fibers spun in methanesulfonic acid with optimized characteristics in the ultrafiltration and nanofiltration range, without requiring the polymer modification. By regulating the temperatures of the coagulation bath and bore fluid, we report hollow fiber membranes with high selectivity for small molecules.

Besides the membrane fabrication, we explore a method of characterization, which allows a detailed analysis of performance and transport mechanism. Frequently, membrane performance characterization is conducted using only dyes or polyglycols, providing restrict information on the potential performance in real applications and feeds, which could be constituted by quite complex mixtures. The main disadvantage of dyes is the risk of adsorption on the membrane, which is even higher when charged dyes and charged polymer surfaces are tested. Polyglycols are classical marker used for membrane performance characterization. With rare exceptions [19], they are mostly linear molecules. Although they are present as coils in solution, under pressure, depending on the interaction with the membrane polymer matrix, their permeance and rejection do not fully represent those of more rigid aromatic molecules relevant for many chemical applications. The characterization of membranes for the separation of hydrocarbons in the petrochemical industry is advancing with the use of more diverse analytical methods [20–22]. Applications in the pharmaceutical sector also require more informative characterization. The hollow fibers produced in this work had varied porosity and were evaluated by introducing a comprehensive method of characterization applying complex mixtures of 23 solutes of diverse size and polarity characteristics. This enables a more accurate evaluation not only of the molecular weight cut off, but also of the membrane capability of separating molecules of similar size and chemistry. The diversity of the solutes employed in this work also provides evidence for a critical analysis of transport mechanism in OSN membranes.

2. Materials and methods

2.1. Materials

The PEEK 450 PF grade from the commercial brand VICTREX® was selected. Methanesulfonic acid (98 %, 96.1 g mol^{-1}), polyethylene glycol (200, 300, 400, 600, 1000, 1500, and 3000 g mol^{-1}), *n*-heptane, toluene, *N*,*N*-dimethylformamide (DMF), acetonitrile, methanol, tetrahydrofuran (THF), *N*,*N*-dimethyactamide (DMAc), chloroform, dimethyl sulfoxide (DMSO) ethanol, sulfuric acid, sodium hydroxide pellets, Chrysodine G (CH), Methyl Red (MR), Methyl Orange (MO), Crystal Violet (CV), Congo Red (CR), Reactive Black 5 (RB5), and Direct Red 80 (DR80) were purchased from Sigma Aldrich. All the chemicals were used without any further purification.

2.2. Spinneret design and manufacture

The 3D-printed spinnerets were produced by stereolithography from Rigid Resin (r) and High Temp Resin V1 (h) by Formlabs [18]. The spinneret has two parts: a body and a cap, as shown in Fig. 1. The body and the cap are secured together using MD POX adhesive by Marston Domsel. The body consists of a round needle to supply bore fluid, supported by horizontal pillars. During the assembly of the body and the cap, an annular gap will form through which the polymer solution will flow. The spinnerets were manufactured using a Formlabs Form 2 stereolithography 3D printer with “Rigid Resin” (r) and “High Temp Resin V1” (h). The printing resolution was 25 μm, with post-processing steps involving washing in 2-propanol and curing under UV light.

2.3. Hollow fiber spinning and module construction

PEEK hollow fibers were prepared by non-solvent induced phase separation (NIPS) process [23–25]. PEEK powder was dried at 80 °C overnight, and methanesulfonic acid was used as a solvent. A 10 wt% dope solution was prepared by mixing PEEK powder and methanesulfonic acid at room temperature with constant stirring. The

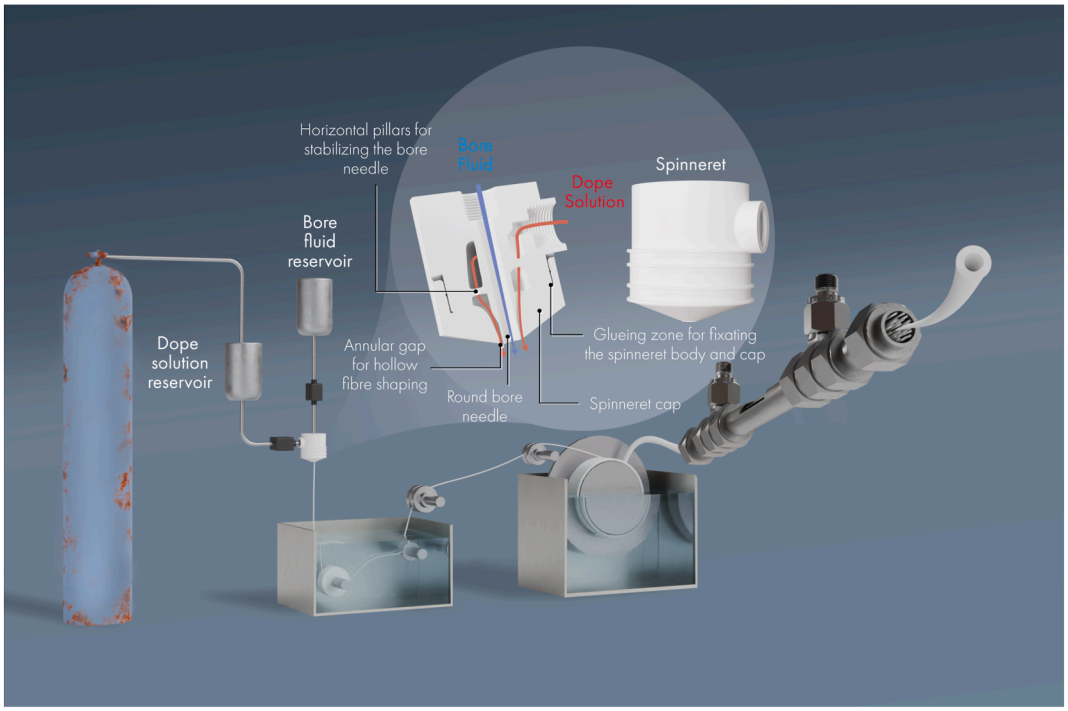

Fig. 1. A cross-sectional view of the 3D-printed spinneret detailing the dimension variables of its orifice, alongside a 25-fiber membrane module of 33 cm effective length and 1 cm diameter.

polymer solution was transferred to the dope solution reservoir and left undisturbed overnight. A spinneret with dimensions of a = 2.2 mm, b = 3.0 mm, and c = 3.6 mm was selected. An upstream pressure of 1.2 bar was maintained in the dope solution reservoir. A bore fluid flow rate of 4 ml min^{-1}, an air gap of 4 cm, and a take-up speed of 20 rotations/min (take-up wheel diameter of 25 cm) were maintained. Water was used as both a coagulation bath and bore fluid. Two sets of spinning were carried out: one with varying bore fluid temperatures (16, 19, 21, 25, and 30 °C) while keeping the coagulation bath at 25 °C, and in the second set, the bore fluid was kept at 25 °C, and the coagulation bath temperature was varied (16, 19, 21, 25, and 30 °C). During spinning, the water in the coagulation bath was constantly stirred as heat was generated at the extruded fiber-water interface. The coagulation bath pH was always maintained above 6.5 as the spinning was conducted with acid. The large volume of the coagulation bath and the addition of ice, when necessary, contributed to a constant and controlled temperature. After spinning the fibers, they were kept in water until the pH value of the water reached 7.0.

As shown in Fig. 1, a hollow fiber module with a fiber length of 33 cm was constructed using Swagelok tubing (stainless steel material, SS316 grade). About 25 fibers were introduced into the module and glued on both sides with an epoxy-based resin. Before constructing the module, the fibers were inspected with an optical microscope for any structural deformities.

2.4. Hollow fiber performance evaluation

The chemical and morphological characterization methods used for the PEEK hollow fibers are described in the Supporting Information.

The performance evaluation was estimated using a custom-made cross-flow setup as shown in Fig. S1 operated at 8 bar and room temperature. The permeance (P) was calculated as:

$$P = \frac{Q}{A\ \Delta P} \tag{1}$$

where Q is the permeate flow rate (L h^{-1}), A is the total hollow fiber active area in the module (m^2), and ΔP is the transmembrane pressure (bar). The permeance of various pure organic solvents (heptane, toluene, *N,N*-dimethylformamide, ethanol, methanol, and acetonitrile) was determined (Table S1).

Dye rejection experiments were performed in DMF using a feed concentration of 30 ppm. The dyes utilized in these filtration studies included Chrysodine G (CH), Methyl Red (MR), Methyl Orange (MO), Crystal Violet (CV), Congo Red (CR), Reactive Black 5 (RB5), and Direct Red 80 (DR80) (Tables S2 and S3). Prior to measuring the dye concentration, the initial 2.5 g of permeate was discarded to ensure accuracy. The dye concentrations in the feed (C_F), permeate (C_P), and retentate (C_R) streams were determined using UV–VIS measurements (NanoDrop 2000c UV–VIS spectrometer, Thermo Scientific). Experiments were performed in triplicate, and dye rejection (R) was calculated as follows:

$$R = 1 - \frac{C_P}{C_F} \tag{2}$$

The molecular weight cutoff of the membranes was estimated using polyethylene glycol (PEG) solutions with molecular weights ranging from 200 to 3000 g mol^{-1} in DMF. The samples were analyzed using gel permeation chromatography with Mixed-H columns at 30 °C. The rejection was calculated using Eq. (2). The molecular weight cutoff was defined as the smallest molecular weight at which the membrane exhibited 90 % rejection.

The performance was further evaluated with a mixture of solutes, including active pharmaceutical ingredients (APIs), aromatic compounds, halogenated aromatics, nitrogen heterocycles, polycyclic aromatic hydrocarbons, and hydrophilic functionalized chemicals (e.g., hydroxyl, amino, methoxy groups) in acetonitrile or DMF at a concentration of 0.25 mM per solute (Tables S2 and S3). After discarding the initial 2.5 g of permeate, concentrations in different streams were analyzed using a high-performance liquid chromatography (HPLC) system (1260 Infinity, Agilent Technologies) equipped with a diode array UV detector and an Eclipse Plus C18 column (150 × 4.6 mm, 3.5 μm, ZORBAX, Agilent Technologies) set at 45 °C. The mobile phase consisted of 0.1 wt% ammonium acetate in LCMS-grade water (A) and HPLC-grade acetonitrile (B), with a run time of 42 min per injection, a 3 μL injection volume, and a hybrid isocratic gradient at a flow rate of 0.6 ml min^{-1}. The detection wavelengths were selected based on the highest absorption for each solute (220, 254, 320, 215, and 232 nm). The data were manually integrated using OpenLab. The concentrations in the feed (C_F), permeate (C_P), and retentate (C_R) were estimated based on the area under the curve for each solute, and the rejection (R) values were calculated using Eq. (2).

The binary separation factor for compound A over compound B was calculated using the following equation:

$$\beta_{A/B} = \frac{C_P^A}{C_F^A} \cdot \frac{C_F^B}{C_P^B} = \frac{1 - R_A}{1 - R_B} \tag{3}$$

To take into account the size differences between the solutes, the binary separation factors were normalized by the ratio of the molecular weights [26]. This is referred to as the selectivity figure of merit ($SFM(\beta_{A/B})$):

$$SFM(\beta_{A/B}) = \frac{\beta_{A/B}}{MW_B/MW_A}, MW_B \,/\, MW_A \geq 1 \tag{4}$$

3. Results and discussion

We successfully developed solvent-stable PEEK hollow fibers using 3D-printed resin-based spinneret. The spinneret enabled the direct spinning of hollow fibers from 10 wt% PEEK dope solutions in methanesulfonic acid, using the set-up depicted in Fig. 1. The optimization of the fabrication conditions led to fibers with tuned porosity for ultra- and nanofiltration. As application, we targeted the concentration and separation of a simulated complex mixture containing molecules with different sizes and chemical functionalization, including APIs and dyes. Hollow fibers are a compact configuration of membranes with a high surface area per volume. The properties of the solvents we considered are listed in Table S1. The mixture components to be separated and their relevance in the pharmaceutical, food and textile industries are listed in Tables S2 and S3.

3.1. Hollow fiber chemical analysis and stability tests

Although methanesulfonic acid is considered milder in terms of potential sulfonation of PEEK when solubilizing, a partial reaction could not be excluded, and a chemical characterization has been conducted to evaluate its extent (Fig. S2). Fourier Transform Infrared (FTIR) spectra (Fig. S2a and S2b) of the hollow fibers revealed peaks at ~3460 cm^{-1} and ~1040 cm^{-1}, which are absent in the pristine PEEK powder. These peaks correspond to O–H vibrations from sulfonic acid groups and symmetric O=S=O stretching [27]. Thermal Gravimetric Analysis (TGA) (Fig. S2c) showed a ~2 % weight loss at ~220 °C for hollow fibers, which could be attributed to a thermal elimination of $–SO_3H$ groups forming SO_2 and water. The primary decomposition temperatures due to the oxidative pyrolysis of the polymer backbone were ~534 °C for hollow fibers and ~565 °C for PEEK powder [28]. Elemental analysis confirmed maximum sulfur mass contents of 0.48 % in the hollow fibers, corresponding to sulfonation degrees of up to 4.6 % (Table S4). The PXRD analysis (Fig. S2d) of the hollow fibers indicate a practical amorphous polymer with interchain distance of 4.7 Å. The XPS analysis (Fig. S3) confirmed a low sulfur content of the spun hollow fiber estimated at 1.32 atomic %. As reported in the literature [29] and confirmed by our experience on sulfonated PEEK for other applications

[30], the solubility in solvents like DMF and DMAc starts to be affected in sulfonation degrees above 40 %.The fiber chemical resistance was tested and confirmed in various solvents (DMF, THF, DMAc, acetonitrile, methanol, heptane, toluene, chloroform, DMSO, concentrated hydrochloric acid, and sodium hydroxide) with no significant changes over 70 days, indicating excellent stability (Table S5).

3.2. *Effect of the bore fluid and coagulation bath temperature on surface characteristics*

The hollow fiber spinning conditions were optimized by changing the temperature of the water used as bore fluid and coagulation bath. Figs. 2 and 3, and Fig. S4–S7 demonstrate the influence of the spinning conditions on the hollow fiber morphology. All fibers have an overall diameter of 1800–1900 μm with a wall thickness of 230 μm and a lumen diameter of 1250–1300 μm. Spinning fibers with a bore fluid and coagulation temperatures of 25 °C, a bore fluid flow rate of 2 ml min^{-1}, and an air gap of 2 cm did not lead to a well-formed lumen. Increasing the air gap to 4 cm and bore fluid flow rate to 4 ml min^{-1} led to an open, well-defined lumen, as seen in Fig. S4 and Fig. S5. Further increases in these parameters did not alter the morphology. The take-up speed and the drum's stretching force significantly affected the dimensions. A higher take-up speed of 20 rotations per minute yielded a lower fiber diameter and thinner walls.

Hollow fibers spun having the coagulation bath and bore fluid at 25 °C had pore sizes in the ultrafiltration range, as can be seen in Figs. 2 and 3 according to the SEM images and the PEG filtration results. However, as the coagulation bath temperature was reduced, the membrane pore size decreased, as reflected in SEM images of the membrane's shell side (Fig. 2 and Fig. S4). A similar trend was observed on the lumen side when the bore fluid temperature was reduced from 25 to 16 °C, while maintaining the coagulation bath at 25 °C (Fig. 3 and Fig. S5). At 16 °C, a smooth skin without visible pores was formed. The SEM images indicate the morphological changes. A detailed evaluation of the pores acting as effective through paths was performed by conducting permeation experiments with solutes of different Stokes radii in dimethylformamide (DMF), as described in the supplementary information text and Table S6. The PEG rejection as a function of Stokes radius is seen in Fig. 2c for fibers prepared with varying coagulation bath temperatures. Lowering the coagulation bath temperature from 25 °C to 16 °C reduced the mean pore size from 38.3 nm to 1.1 nm (Fig. 2d). Fig. 3c shows the rejection for fibers prepared with different bore fluid temperatures. The mean pore size decreased from 44.9 nm to 0.6 nm when the bore fluid temperature dropped from 25 °C to 16 °C (Fig. 3d). In summary, membranes prepared with coagulation bath and bore fluid at 25 °C have pores in the ultrafiltration range. As the preparation temperature lowers down to 19 and 16 °C, a more selective skin is built on the low temperature side, forming membranes suitable for nanofiltration. The pore size has obvious implications in the hollow fiber separation and transport performances, which are discussed in the next section.

Controlling the pore size distribution by changing the bore fluid temperature is more effective than adjusting the coagulation bath temperature, since the volume of the bore fluid is smaller. Cross-sectional images of fibers spun at varying coagulation bath temperatures (16–25 °C) while keeping bore fluid constant at 25 °C are shown in Fig. S6. Similar images show fibers spun with a constant coagulation bath temperature of 25 °C, changing bore fluid temperatures (Fig. S7).

The effect of the temperature on the pore formation can be

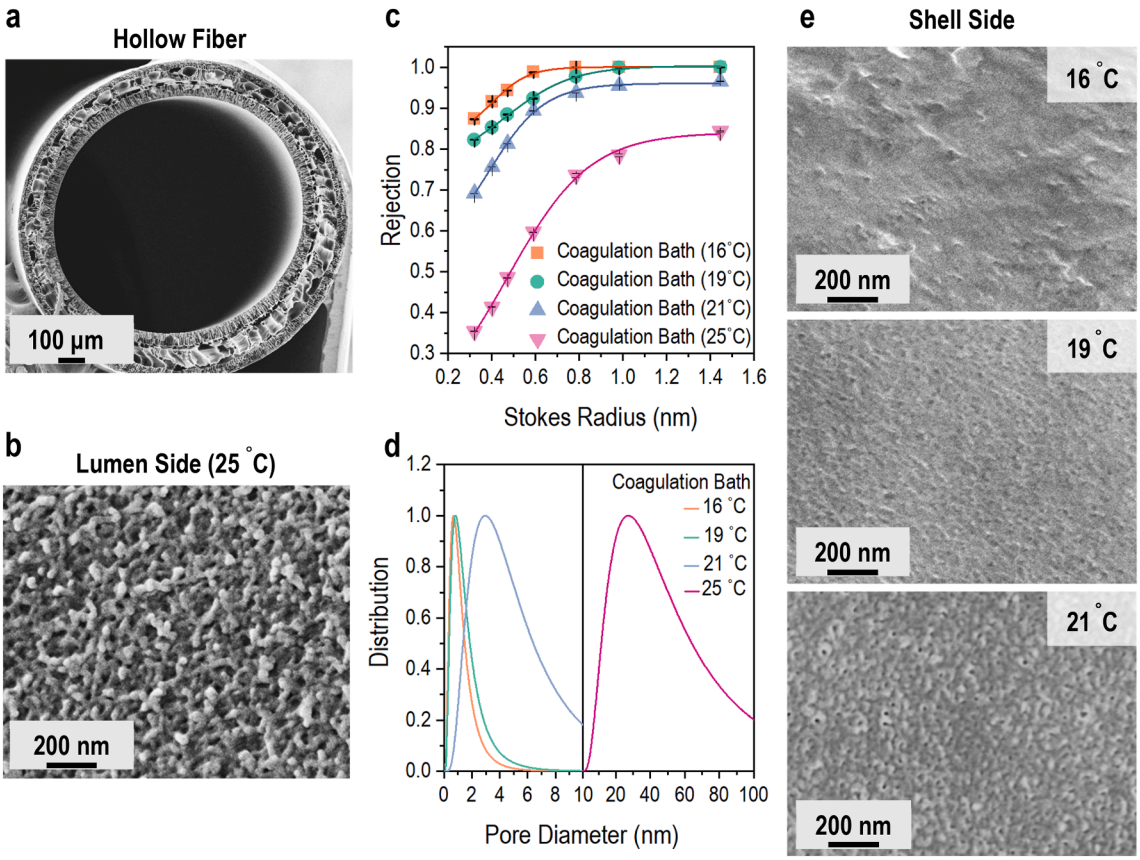

Fig. 2. Effect of coagulation bath temperature. SEM images and pore size distribution of hollow fibers spun from 10 wt% PEEK in methanesulfonic acid with a 4 cm air gap, a 4 ml min^{-1} bore fluid flow rate at 25 °C, and a take-up speed of 20 rotations per minute. (a) Cross-section and (b) lumen surface morphology. (c) Rejection curves for PEG with different Stoke radii in DMF. (d) Pore size distribution. (e) Shell surface morphology of fibers prepared with different coagulation bath temperatures.

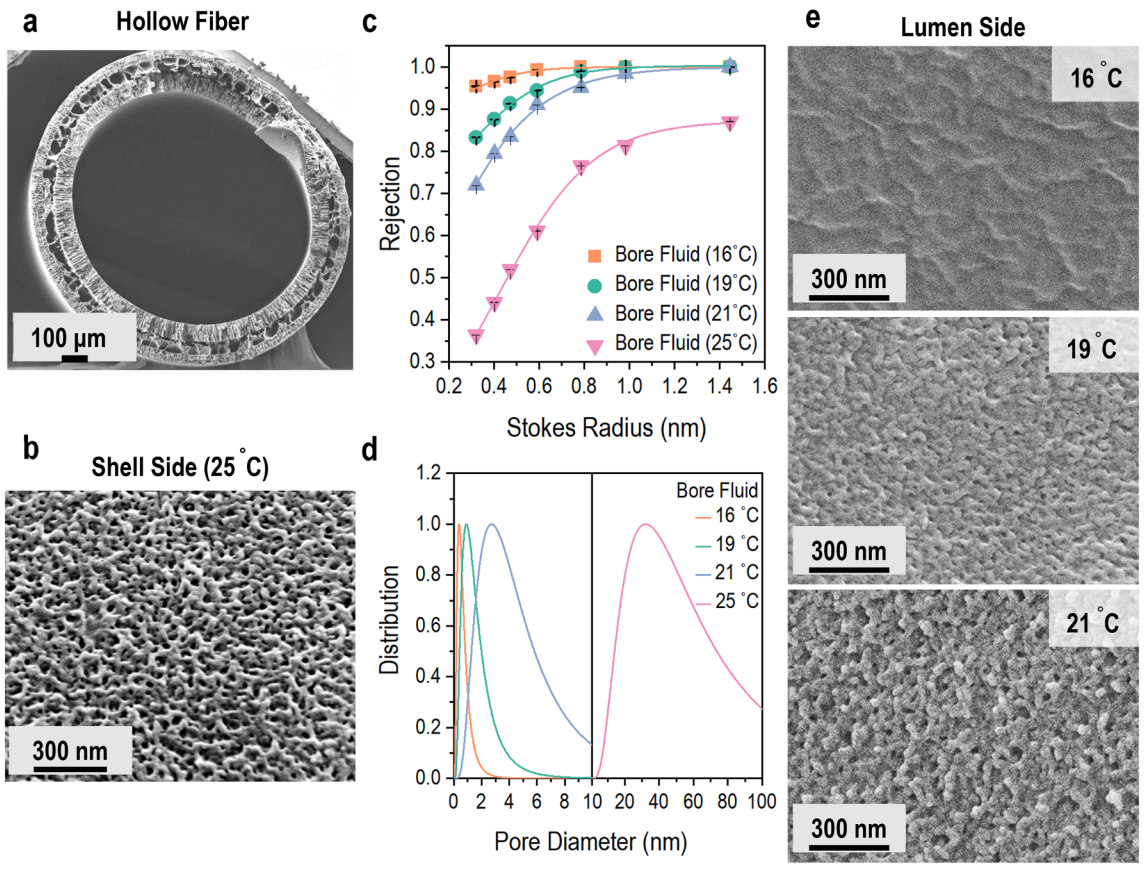

Fig. 3. Effect of bore fluid temperature. SEM images and pore size distribution of hollow fibers spun from 10 wt% PEEK in methanesulfonic acid with a 4 cm air gap, a bore fluid flow rate of 4 ml min^{-1}, a take-up speed of 20 rotations per minute, and a coagulation bath temperature of 25 °C. (a) Cross-section and (b) shell surface morphology. (c) Rejection curves for PEG with different Stoke radii. (d) Pore size distribution in DMF. (e) Lumen surface morphology of fibers prepared with different bore fluid temperatures.

summarized as follows. The pores in the membrane selective layer are the result of a phase separation in the dope solution induced by the solvent-nonsolvent exchange with the bore fluid and coagulation bath. Typically for systems like the one reported in this work, the phase separation follows the spinodal decomposition mechanism. Local composition oscillations initiate and progress with increasing intensity and amplitude [31]. The polymer-lean phase gives rise to the pores. The phase separation continues until the viscosity of the polymer-rich phase becomes high enough to practically solidify and immobilize the pore structure. A low temperature promotes the solidification at earlier stages and slows down the phase separation progress. The resulting pores are therefore smaller.

3.3. Solvent transport through PEEK hollow fibers

By adjusting the bore fluid or coagulation bath temperature, the porosity and selectivity of the membranes were optimized. The DMF permeance (Eq. (1)) was quantified and the selectivity was initially evaluated using dyes and PEG of different molecular weights in DMF (Figs. 2 and 3, Fig. S8). The molecular weight cut-off (MWCO), the minimum size of molecules with 90 % rejection (Eq. (2)), was influenced by the preparation temperatures. Membranes prepared at 25°C rejected 86 % PEG 3000, indicating that the MWCO would be slightly above 3000 g mol^{-1}, and therefore in the ultrafiltration range. By reducing the temperature of bore fluid or coagulation bath, the membrane selectivity increased, with the highest rejection values achieved at 16 °C. The MWCO decreased to 270 g mol^{-1} as the coagulation bath temperature was lowered to 16 °C. Reducing the bore fluid temperature to 16 °C was even more effective (Figs. 2 and 3).

The DMF permeances of the hollow fibers prepared under different bore fluid and coagulation bath temperatures are shown in Fig. S9. The permeance decreases as the bore fluid or coagulation bath temperature decreases, the lowest value being 0.9 L m^{-2} h^{-1} bar^{-1}. The permeance values are competitive with those reported in the literature for other hollow fibers (Table S8), [16,18,32,33,52–96].

Figs. S10S12 show how the DMF permeance is affected by the testing temperature and corresponding change of permeant viscosity. This effect suggests at first sight that the transport could follow the pore-flow mechanism. However, when prepared at 16 and 19°C, the mechanism of transport through these membranes might be more complex and justified a more detailed investigation (Fig. 4).

We evaluated the permeance of a series of solvents with different physicochemical properties (Table S1) through PEEK hollow fibers (Fig. 4 and Fig. S13) and analyzed the transport based on the models of pore-flow, solution-diffusion, and solution-friction. A brief description of these models is presented in the supporting information [34–36]. The transport mechanism in nanofiltration membranes of different materials prepared by nonsolvent induced phase separation, dip coating, and interfacial polymerization has been the topic of a lively discussion in the literature, with strong arguments supported by experimental and theoretical modeling [37–43]. Here we fit the permeance results with the core parameters highlighted in the different mechanism models. The analysis is purely based on experimental measurements and focused on the PEEK membranes developed in this work without extending it to other kinds of membranes.

According to the pore-flow model, the solvent transport through membranes is pressure-driven. The permeance depends on the inverse of the solvent viscosity and the square of the membrane pore radius,

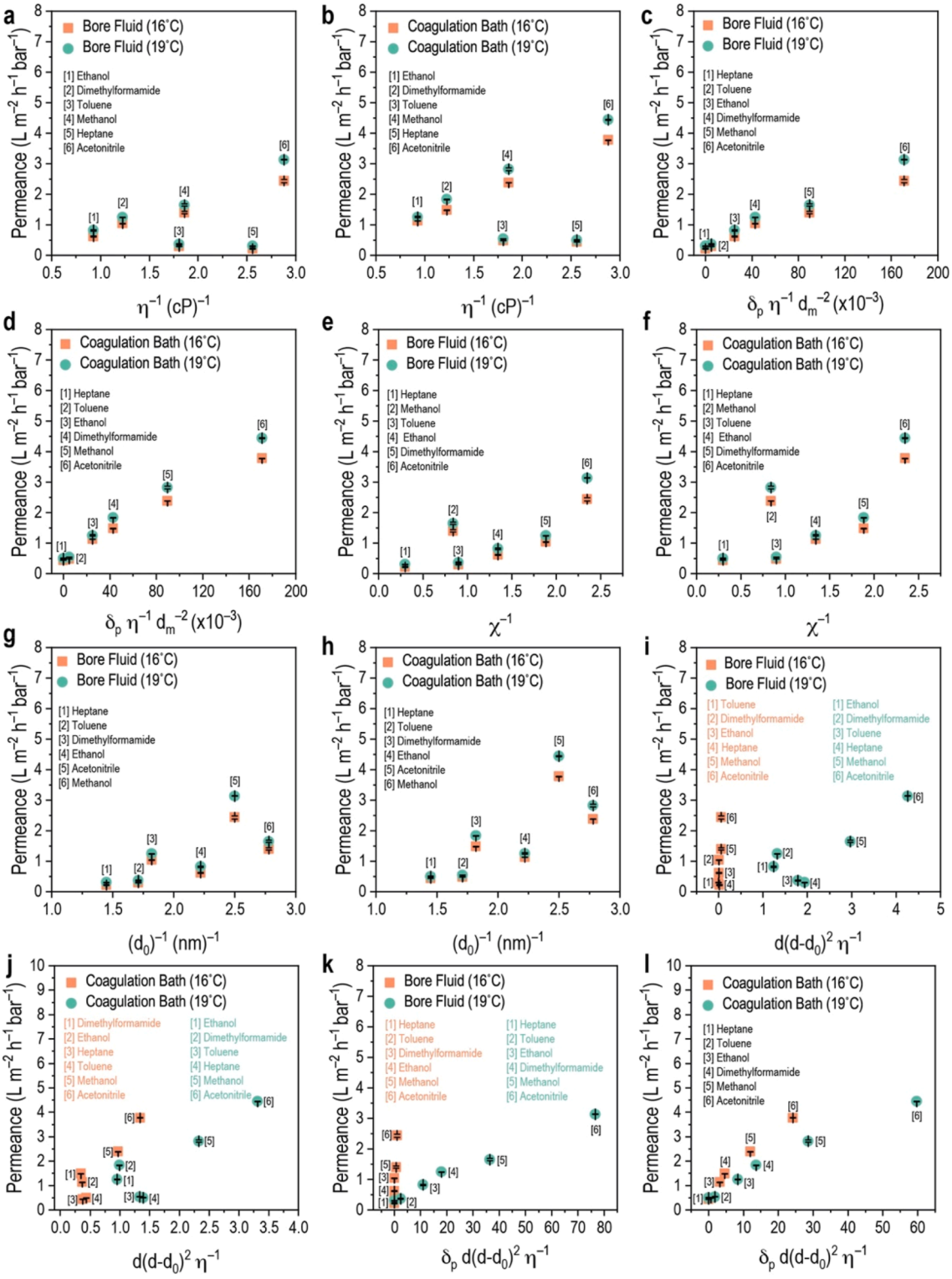

Fig. 4. The permeance data is plotted against core parameters derived from pore flow, solution diffusion, and solution friction models. The analysis includes solvent properties such as viscosity (η), molar diameter (d_m), kinetic diameter (d_0), polar solubility contribution (δ_P), along with material-specific parameters like Flory-Huggins interaction parameter (χ) and membrane pore-size (d). Linear regression trends with corresponding R^2 values are indicated where applicable.

following the Hagen-Poiseuille equation. Plots of solvent permeances as a function of the inverse of their viscosity show some linear correlation for polar solvents (Fig. 4a and b). However, nonpolar solvents like toluene and heptane significantly deviate from the linearity, indicating that solvent polarity affects the transport mechanism of PEEK membranes even when pores are large.

In the solution-diffusion (or sorption-diffusion) model, the thermodynamic affinity between permeants and the membrane material is a primary factor for the transport. The chemical potential gradient, or the permeant activity difference across the membrane, promoted by the applied pressure difference, is the driving force [43]. The solvent permeance depends on its solubility, particularly in non-porous or dense

membranes. A balance of solubility and diffusivity controls the transport. To evaluate how our results fit this model, we plotted permeance as a function of combined solvent properties, taking into account the polar contribution to the solubility parameters (δ_P), viscosity (η), and molar diameter (d_m) (Fig. 4c–d) [44]. This better matched our experimental data than the pure pore flow model, especially for membranes spun in various coagulation bath temperatures with bore fluid at 25 °C. However, δ_P is a permeant characteristic and therefore the expression in Fig. 4c–d only considers solvent properties, neglecting those of the membrane.

To better reflect the membrane-solvent interactions, we plotted permeance against the Flory-Huggins interaction parameter (χ), indicating solvent-polymer affinity (Fig. 4e–f and Table S7). A high polymer-solvent affinity (small χ) correlated with increased permeance, suggesting that solvent-polymer interactions are relevant for the transport.

Recent studies using non-equilibrium molecular dynamics (MD) simulations have challenged the adequacy of the solution-diffusion model in fully explaining the solvent transport through membranes, particularly for systems with porous structures [40,45,46]. These studies suggest that convective pore flow predominantly governs transport, with solvent molecules moving as clusters through interconnected channels. We tested these findings against experimental data from PEEK hollow fibers with varying skin layer characteristics.

The pore flow model requires that the solvent permeance would linearly increase with the inverse of the solvent kinetic diameter. However, our data deviates from this linearity (Fig. 4g–h), indicating that the transport through PEEK membranes does not solely rely on size exclusion. We examined correlations proposed by the solution-friction model [47], and considered transport driven by pressure gradients [40,46]. This correlation, based on the energy barrier required for solvent transport through nanopores, proposes that permeance is proportional to the square of the difference between the membrane pore size (d) and solvent kinetic diameter (d_0) multiplied by the pore size and inversely proportional to the solvent viscosity (η). We plotted the solvent permeance as a function of $d(d-d_0)^2\eta^{-1}$ and $\delta_P d(d-d_0)^2\eta^{-1}$ (Fig. 4i–l). Deviations from linearity were observed (Fig. 4i–j and Fig. S13a). A more linear correlation was observed with $\delta_P d(d-d_0)^2\eta^{-1}$ (Fig. 4k–l). This suggests that the solvent affinity to the membrane might have a contribution, besides size and friction. Fig. S14 shows plots of permeance as a function of $\delta_P d(d-d_0)^2\chi^{-1}$, similar to Fig. 4k–l, but considering the thermodynamic interaction between permeant and membrane polymer material instead of the polarity of the permeant alone. The correlation follows a clear trend, but the linearity in Fig. 4k–l (with δ_P) for the investigated system was better. Although we consider the proposed plots in Fig. S14 a relevant approach, there are limitations in the availability of precise χ measured values. The values of χ were estimated as described in the supplementary information, based on differences between total solubility parameter values of the membrane polymer and the permeant. This is a practical and simplified equation but does not include factors such as concentration dependence and more specific enthalpic and entropic considerations, which might be relevant [48].

3.4. Active pharmaceutical ingredients (APIs) separations

The selectivity of PEEK hollow fibers for a mixture of APIs and other molecules (Table S2) with different sizes and chemical characteristics was then evaluated. The overall rejection increased as the bore fluid and coagulation bath temperatures decreased. This increase is due to the denser skin layer formed at lower temperatures. Fig. 5a–b and Fig. 15a and b reflect the influence of solute size on the rejection. The rejections of 23 components of a complex mixture were plotted as a function of van der Waals volume and molecular weight, respectively, as analyzed by HPLC. Particularly for fibers spun with the bore fluid at 25 °C (Fig. 5b), a trend typical of size separation mechanism was observed. These are fibers with larger lumen pores and a more open selective layer. The rejections of larger molecules like rifaximin (RFX, 785.9 g mol^{-1}, 435.7 cm^3 mol^{-1}) and rifampicin (RIF, 823 g mol^{-1}, 471.4 cm^3 mol^{-1}) were above 90 %, independent of the coagulation bath temperature. The rejections of markers smaller than 200 cm^3 mol^{-1} become clearly lower as the coagulation temperature increases. Membranes prepared with a coagulation bath at 25°C and bore fluids at temperatures 16 and 19°C, had a higher rejection in a comparable van der Waals volume range.

However, there are deviations from the pure size effect, which are more evident in membranes prepared at lower bore fluid temperature. A first example is the rejection of solutes containing heavy elements, such as 4-iodoanisole (4IA), which slightly deviates from that of molecules with similar molecular weights [49]. A second example is the fact that, although octocrylene (OCT) and dipyridamole (DIPY) are larger than triptycene (TRP), their rejection rates were slightly lower. Similarly, 4 MA exhibited higher rejection than DMP despite their similar sizes. These deviations indicate that other factors beyond molecular size also influence the rejection behavior. Fig. 5c highlights the impact of several molecular descriptors on the solute rejection for membranes with denser selective layer fabricated at 19 °C bore fluid and 25 °C coagulation bath. The solute hydrophobicity, expressed by the LogP value, significantly influenced the rejection behavior. Hydrophobic solutes like TRP had high rejection values, likely due to lower solubility in hydrophilic membrane areas, impeding the transport. Solutes with lower polar contributions to the Hansen solubility parameter had larger rejection, reinforcing the role of polarity in membrane-solute interactions (Fig. 5c and Fig. S15c–d). The Flory-Huggins interaction parameter (χ), which indicates solute-polymer miscibility, was particularly notable in differentiating the behavior of solutes with similar sizes, as seen with 4 MA and DMP (Tables S5 and S6). 4 MA-PEEK interactions have a higher χ value and this contributes to a higher rejection than DMP despite similar sizes. This suggests membrane performance is mainly governed by size exclusion, but with additional influences from solute physicochemical properties.

For membranes prepared with bore fluid at 19°C, similar rejection values were obtained in DMF and acetonitrile for solutes larger than 234 g mol^{-1} (Fig. S16 and Fig. S17). As expected, the differences are more evident for smaller molecules. In this case, the rejection efficiency was generally higher for solutes in acetonitrile than in DMF, likely due to different solvent-membrane interactions causing slight swelling.

The long-term stability of PEEK hollow fibers in a challenging solvent like DMF (Fig. S17a). Although rejection of small molecules (DMP and 4 MA) near 120 g mol^{-1} was slightly affected, larger solutes like RIF and RFX maintained high rejection. The DMF permeance remained stable with maximum variation around 20 % variation over 14 days. Overall, the rejection and permeance values suggested that the membrane's integrity was preserved through filtration.

Plots of rejection as a function of molecular weight or van der Waals volumes like Fig. 5a and b, S15a and S15b are a good and simple indication of the membrane potential, when considering the following applications: (i) concentration of solutes of a certain size; (ii) separation from impurities of significantly different sizes; (iii) recycling of solvents used for a purification process.

When the target application is the separation of molecules of similar size and properties in a complex mixture, Fig. 5d provides a much better visualization. Similar to the approach recently applied to interfacial polymerization membranes [49], the figure depicts a matrix of pairwise selectivity ratios, normalized by their corresponding molecular weights (Eqs. (3) and (4)). These values are known as “selectivity figure of merit”. The matrix in Fig. 5d was built using a feed containing 23 solutes dissolved in DMF. The complex feed and permeant solutions were analyzed by HPLC. The membrane was fabricated with a 19 °C bore fluid and 25 °C coagulation bath. In summary, the matrix shows for each pair of molecules the predicted efficiency for their separation. Higher potential of separation is indicated by larger values. A scale in colors highlights and differentiates higher values in green and yellow from low

values in blue. For instance, large molecules like RFX can be more easily separated from smaller ones like CG but would be hardly separated (values closer to 1) from those of similar sizes like DIPY. Besides size, more hydrophobic solutes, such as TRP would have higher selectivity over hydrophilic ones like caffeine (CAF), indicating the importance of hydrophobic interactions.

Figs. S18 and S19 show a different way of representing selectivity. It plots the logarithmic correlation between the binary separation factor $\left(\beta_{A/B}\right)$ for molecules A and B (calculated by eq. (3)) and the rejection of the less permeable molecule (R_B). The data points are distributed along a diagonal grid; each line represents the potential separation of one marker from a series of others. The rejection values in this case are between 0 and 1 (corresponding to 0 and 100 %). As the rejection of B increases, $\log(1\text{-}R_B)$ becomes less negative and the values of $\log\left(\beta_{A/B}\right)$ decline [50,51]. In summary, a broader distribution of points in the x-y plane indicates a greater ability to separate solutes with similar characteristics, thereby enhancing the overall rejection selectivity of the membrane. In other words, the larger the area covered by the measured points, the higher the overall selectivity of the membrane. The curves of RFX and RIF are practically overlapped and clearly separated from other tested molecules depicted in Fig. S18 for all membranes. Analogous plots in Fig. S19 are for PEG with different sizes. In this case, the permeants differ only by size. The distinction between hollow fibers spun under different conditions is clearer. The separation between components is more effective with fibers spun at lower temperatures. A notable difference is seen by reducing the bore fluid temperature from 25 to 21 °C, while keeping the coagulation bath at 25 °C.

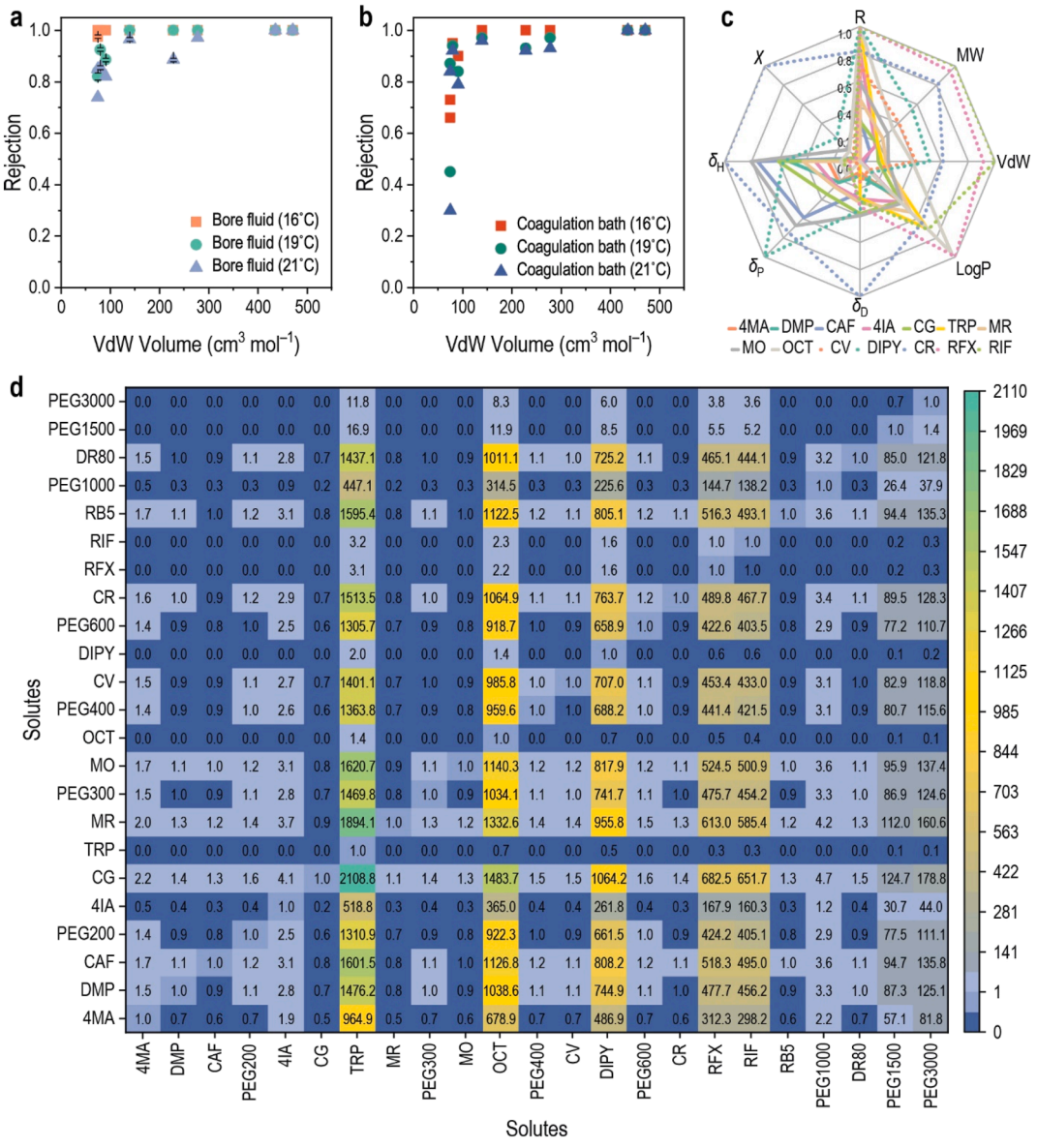

Fig. 5. Rejection of solutes with diverse functionalities, including active pharmaceutical ingredients (APIs), dissolved in acetonitrile, by membranes prepared at different (a) bore fluid and (b) coagulation bath temperatures, plotted as a function of van der Waals volume (VdW). (c) Influence of solute physicochemical properties on membrane rejection behavior for membranes prepared with a bore fluid temperature of 19 °C and a coagulation bath temperature of 25 °C. Parameters analyzed include molecular weight (MW), Van der Waals volume (VdW), Flory-Huggins interaction parameter (χ), LogP, and the contributions to Hansen solubility parameters: dispersion forces (δ_D), polar interactions (δ_P), and hydrogen bonding (δ_H). The rejection of solutes was carried out in DMF. (d) Rejection selectivity matrix for 23 different solutes dissolved in DMF for membranes prepared with a bore fluid temperature of 19 °C and a coagulation bath temperature of 25 °C. The matrix presents pairwise selectivity ratios, highlighting separation capabilities across a range of solutes based on membrane performance.

4. Conclusion

We demonstrated the separation of a complex mixture of 23 API components using PEEK hollow fibers fabricated by a solution process at room temperature using acid-stable spinnerets. The spinning conditions were optimized by adjusting the bore fluid and coagulation bath temperatures from 16 to 25 °C. Lower temperatures reduced the pore size and created a denser skin layer, enhancing selectivity in nanofiltration and reverse osmosis. Acetonitrile permeances of 3 L m^{-2} h^{-1} bar^{-1} and DMF permeances between 0.9 and 2.2 L m^{-2} h^{-1} bar^{-1} were obtained. A critical analysis of the solvent transport mechanism indicated a predominance of pore flow (permeance $\propto\eta^{-1}$) for polar solvents through fibers spun with bore fluid at 25 °C. However, toluene and heptane have a strong deviation. For fibers spun at lower bore fluid temperatures, we proposed better correlations by plotting permeance as a function of $\delta_p d(d-d_0)^2\eta^{-1}$, and $\delta_P d(d-d_0)^2\chi^{-1}$, which consider the effect of solvent polarity, viscosity, and the difference between the solvent kinetic diameter and the membrane pore size, therefore considering affinity and friction. A rejection selectivity matrix for all components mixture was calculated for hollow fibers spun with a bore fluid temperature of 19 °C and a coagulation bath temperature of 25 °C. By adjusting spinning conditions, we tailored the separation performance, achieving high rejection rates for small solutes around 100 g mol^{-1}, demonstrating potential applications in solvent recovery and API concentration.

CRediT authorship contribution statement

Banan Alhazmi: Writing – original draft, Methodology, Formal analysis, Conceptualization. **Lakshmeesha Upadhyaya:** Writing – original draft, Methodology, Investigation, Formal analysis, Data curation, Conceptualization. **Shanshan Hong:** Methodology. **Gergo Ignacz:** Methodology. **Radosław Górecki:** Methodology. **Maik Tepper:** Methodology. **Hannah Roth:** Methodology. **Matthias Wessling:** Supervision, Funding acquisition, Conceptualization. **Gyorgy Szekely:** Supervision, Methodology. **Suzana P. Nunes:** Writing – review & editing, Supervision, Funding acquisition, Conceptualization.

Conflict of interest

The authors of the manuscript declare no conflict of interest.

Acknowledgments

The authors thank King Abdullah University of Science and Technology (KAUST) for Research Funding. Fig.1 and the graphical abstract were produced by Ana Bigio, scientific illustrator.

Appendix A. Supplementary data

Supplementary data to this article can be found online at https://doi.org/10.1016/j.advmem.2025.100193.

Data availability

All data that support the findings of this study are available within the paper and Supporting Information files or from the corresponding author upon request.

References

[1] G. Szekely, M.F. Jimenez-Solomon, P. Marchetti, J.F. Kim, A.G. Livingston, Sustainability assessment of organic solvent nanofiltration: from fabrication to application, Green Chem. 16 (10) (2014) 4440–4473, https://doi.org/10.1039/C4GC00701H.

[2] H. Xiao, Y. Feng, W.R.F. Goundry, S. Karlsson, Organic solvent nanofiltration in pharmaceutical applications, Org. Process Res. Dev. 28 (4) (2024) 891–923, https://doi.org/10.1021/acs.oprd.3c00470.

[3] P. Marchetti, M.F. Jimenez Solomon, G. Szekely, A.G. Livingston, Molecular separation with organic solvent nanofiltration: a critical review, Chem. Rev. 114 (21) (2014) 10735–10806, https://doi.org/10.1021/cr500006j.

[4] M. Galizia, K.P. Bye, Advances in organic solvent nanofiltration rely on physical chemistry and polymer chemistry, Front. Chem. 6 (511) (2018), https://doi.org/10.3389/fchem.2018.00511.

[5] S.L. Aristizábal, R.P. Lively, S.P. Nunes, Solvent and thermally stable polymeric membranes for liquid molecular separations: recent advances, challenges, and perspectives, J. Membr. Sci. 685 (2023) 121972, https://doi.org/10.1016/j.memsci.2023.121972.

[6] D.J. Kemmish, J.N. Hay, The effect of physical ageing on the properties of amorphous PEEK, Polymer 26 (6) (1985) 905–912, https://doi.org/10.1016/0032-3861(85)90136-3.

[7] A.M. Díez-Pascual, G. Martínez, M.A. Gómez, Synthesis and characterization of Poly(ether ether ketone) derivatives obtained by carbonyl reduction, Macromolecules 42 (18) (2009) 6885–6892, https://doi.org/10.1021/ma901208e.

[8] Y. Ding, B. Bikson, Preparation and characterization of semi-crystalline poly(ether ether ketone) hollow fiber membranes, J. Membr. Sci. 357 (1) (2010) 192–198, https://doi.org/10.1016/j.memsci.2010.04.021.

[9] S. Li, T.J. Pyrzynski, N.B. Klinghoffer, T. Tamale, Y. Zhong, J.L. Aderhold, S. James Zhou, H.S. Meyer, Y. Ding, B. Bikson, Scale-up of PEEK hollow fiber membrane contactor for post-combustion CO2 capture, J. Membr. Sci. 527 (2017) 92–101, https://doi.org/10.1016/j.memsci.2017.01.014.

[10] T. Huang, G. Chen, Z. He, J. Xu, P. Liu, Pore structure and properties of poly(ether ether ketone) hollow fiber membranes: influence of solvent-induced crystallization during extraction, Polym. Int. 68 (11) (2019) 1874–1880, https://doi.org/10.1002/pi.5897.

[11] M.F. Sonnenschein, Hollow fiber microfiltration membranes from poly(ether ether ketone) (PEEK), J. Appl. Polym. Sci. 72 (2) (1999) 175–181, https://doi.org/10.1002/(SICI)1097-4628(19990411)72:2.

[12] J. da Silva Burgal, L. Peeva, A. Livingston, Towards improved membrane production: using low-toxicity solvents for the preparation of PEEK nanofiltration membranes, Green Chem. 18 (8) (2016) 2374–2384, https://doi.org/10.1039/C5GC02546J.

[13] J. da Silva Burgal, L. Peeva, A. Livingston, Negligible ageing in poly(ether-ether-ketone) membranes widens application range for solvent processing, J. Membr. Sci. 525 (2017) 48–56, https://doi.org/10.1016/j.memsci.2016.10.015.

[14] J. da Silva Burgal, L. Peeva, P. Marchetti, A. Livingston, Controlling molecular weight cut-off of PEEK nanofiltration membranes using a drying method, J. Membr. Sci. 493 (2015) 524–538, https://doi.org/10.1016/j.memsci.2015.07.012.

[15] J. da Silva Burgal, L.G. Peeva, S. Kumbharkar, A. Livingston, Organic solvent resistant poly(ether-ether-ketone) nanofiltration membranes, J. Membr. Sci. 479 (2015) 105–116, https://doi.org/10.1016/j.memsci.2014.12.035.

[16] S.L. Aristizábal, L. Upadhyaya, G. Falca, A.Y. Gebreyohannes, M.O. Aijaz, M. R. Karim, S.P. Nunes, Acid-free fabrication of polyaryletherketone membranes, J. Membr. Sci. 660 (2022) 120798, https://doi.org/10.1016/j.memsci.2022.120798.

[17] S.L. Aristizábal, S. Chisca, B.A. Pulido, S.P. Nunes, Preparation of PEEK membranes with excellent stability using common organic solvents, Ind. Eng. Chem. Res. 59 (12) (2020) 5218–5226, https://doi.org/10.1021/acs.iecr.9b04281.

[18] S.L. Aristizábal, L. Upadhyaya, M. Tepper, H. Roth, M. Ramírez-Martínez, M. Wessling, S.P. Nunes, Poly(aryl ether ketone) hollow fibers preparation with acid resistant spinnerets, J. Membr. Sci. 674 (2023) 121436, https://doi.org/10.1016/j.memsci.2023.121436.

[19] A. Yushkin, R. Borisov, V. Volkov, A. Volkov, Improvement of MWCO determination by using branched PEGs and MALDI method, Separ. Purif. Technol. 211 (2019) 108–116.

[20] Y.J. Lee, H.Y. Jang, B.D. Marshall, M.I. Abutaqiya, N. Rangnekar, N.C. Bruno, M. Finn, R.P. Lively, Fractionation of complex aromatic hydrocarbon mixtures using membrane cascades hybridized with distillation, Chem. Eng. J. 503 (2025) 158170.

[21] S. Chisca, V.-E. Musteata, W. Zhang, S. Vasylevskyi, G. Falca, E. Abou-Hamad, A.-H. Emwas, M. Altunkaya, S.P. Nunes, Polytriazole membranes with ultrathin tunable selective layer for crude oil fractionation, Science 376 (6597) (2022) 1105–1110, https://doi.org/10.1126/science.abm76.

[22] S. Chisca, M.N. Hedhili, V.G. Samaras, J. Liu, S.P. Nunes, Sour to sweet crude oil with membranes, J. Membr. Sci. 701 (2024) 122716.

[23] A.Y. Gebreyohannes, L. Upadhyaya, L.P. Silva, G. Falca, P.J. Carvalho, S.P. Nunes, Hollow fibers with encapsulated green amino acid-based ionic liquids for dehydration, ACS Sustain. Chem. Eng. 8 (48) (2020) 17763–17771, https://doi.org/10.1021/acssuschemeng.0c06001.

[24] L. Upadhyaya, A.Y. Gebreyohannes, F.H. Akhtar, G. Falca, V. Musteata, D. K. Mahalingam, R. Almansoury, K.C. Ng, S.P. Nunes, NEXARTM-coated hollow fibers for air dehumidification, J. Membr. Sci. 614 (2020) 118450, https://doi.org/10.1016/j.memsci.2020.118450.

[25] L. Upadhyaya, A.Y. Gebreyohannes, M.W. Shahzad, U.T. Syed, S.L. Aristizábal, R. Gorecki, S.P. Nunes, Polyphenol-coated hollow fiber system for energy-efficient dehumidification in air-conditioning, J. Membr. Sci. 692 (2024) 122215, https://doi.org/10.1016/j.memsci.2023.122215.

[26] P. Marchetti, L. Peeva, A. Livingston, The selectivity challenge in organic solvent nanofiltration: membrane and process solutions, Annu. Rev. Chem. Biomol. Eng. 8 (1) (2017) 473–497, https://doi.org/10.1146/annurev-chembioeng-060816-101325.

[27] P. Xing, G.P. Robertson, M.D. Guiver, S.D. Mikhailenko, K. Wang, S. Kaliaguine, Synthesis and characterization of sulfonated poly(ether ether ketone) for proton

exchange membranes, J. Membr. Sci. 229 (1) (2004) 95–106, https://doi.org/10.1016/j.memsci.2003.09.019.
[28] P. Knauth, H. Hou, E. Bloch, E. Sgreccia, M.L. Di Vona, Thermogravimetric analysis of SPEEK membranes: thermal stability, degree of sulfonation and cross-linking reaction, J. Anal. Appl. Pyrolysis 92 (2) (2011) 361–365, https://doi.org/10.1016/j.jaap.2011.07.012.
[29] R. Huang, P. Shao, C. Burns, X.-s. Feng, Sulfonation of poly (ether ether ketone) (PEEK): kinetic study and characterization, J. Appl. Polym. Sci. 82 (11) (2001) 2651–2660.
[30] S. Vetter, B. Ruffmann, I. Buder, S. Nunes, Proton conductive membranes of sulfonated poly (ether ketone ketone), J. Membr. Sci. 260 (1–2) (2005) 181–186.
[31] S.P. Nunes, T. Inoue, Evidence for spinodal decomposition and nucleation and growth mechanisms during membrane formation, J. Membr. Sci. 111 (1) (1996) 93–103.
[32] Y. Li, B. Cao, P. Li, Effects of dope compositions on morphologies and separation performances of PMDA-ODA polyimide hollow fiber membranes in aqueous and organic solvent systems, Appl. Surf. Sci. 473 (2019) 1038–1048, https://doi.org/10.1016/j.apsusc.2018.12.245.
[33] K.Y. Wang, B. Li, T.-S. Chung, 3D-macrocycles impregnated polybenzimidazole hollow fiber membranes with excellent organic solvent resistance for industrial solvent recovery, J. Membr. Sci. 638 (2021) 119678, https://doi.org/10.1016/j.memsci.2021.119678.
[34] O. Kedem, A. Katchalsky, Thermodynamic analysis of the permeability of biological membranes to non-electrolytes, Biochim. Biophys. Acta 27 (1958) 229–246, https://doi.org/10.1016/0006-3002(58)90330-5.
[35] P.M. Biesheuvel, Two-fluid model for the simultaneous flow of colloids and fluids in porous media, J. Colloid Interface Sci. 355 (2) (2011) 389–395, https://doi.org/10.1016/j.jcis.2010.12.006.
[36] R.W. Baker, Membrane Technology and Applications, John Wiley & Sons2012.
[37] J.G. Wijmans, R.W. Baker, The solution-diffusion model: a review, J. Membr. Sci. 107 (1–2) (1995) 1–21, https://doi.org/10.1016/0376-7388(95)00102-I.
[38] V. Freger, G.Z. Ramon, The solution-diffusion model: “Rumors of my death have been exaggerated”, J. Membr. Sci. Lett. 4 (2) (2024) 100084 https://doi.org/10.1016/j.memlet.2024.100084.
[39] H. Fan, M. Heiranian, M. Elimelech, The solution-diffusion model for water transport in reverse osmosis: what went wrong? Desalination 580 (2024) 117575 https://doi.org/10.1016/j.desal.2024.117575.
[40] L. Wang, J. He, M. Heiranian, H. Fan, L. Song, Y. Li, M. Elimelech, Water transport in reverse osmosis membranes is governed by pore flow, not a solution-diffusion mechanism, Sci. Adv. 9 (15) (2023) eadf8488, https://doi.org/10.1126/sciadv.adf8488.
[41] R. Sujanani, K.K. Reimund, K.L. Gleason, B.D. Freeman, Hydraulic permeation-induced water concentration gradients in ion exchange membranes, J. Membr. Sci. 705 (2024) 122858, https://doi.org/10.1016/j.memsci.2024.122858.
[42] P. Marchetti, A.G. Livingston, Predictive membrane transport models for Organic Solvent Nanofiltration: how complex do we need to be? J. Membr. Sci. 476 (2015) 530–553, https://doi.org/10.1016/j.memsci.2014.10.030.
[43] J. Wijmans, Permeation experiments reveal the mechanism of membrane permeation, J. Membr. Sci. (2025) 124607, https://doi.org/10.1016/j.memsci.2025.124607.
[44] S. Karan, Z. Jiang, A.G. Livingston, Sub-10 nm polyamide nanofilms with ultrafast solvent transport for molecular separation, Science 348 (6241) (2015) 1347–1351, https://doi.org/10.1126/science.aaa5058.
[45] H. Fan, J. He, M. Heiranian, W. Pan, Y. Li, M. Elimelech, The physical basis for solvent flow in organic solvent nanofiltration, Sci. Adv. 10 (24) (2024), https://doi.org/10.1126/sciadv.ado4332 eado4332.
[46] J. He, H. Fan, M. Elimelech, Y. Li, Molecular simulations of organic solvent transport in dense polymer membranes: solution-diffusion or pore-flow mechanism? J. Membr. Sci. 708 (2024) 123055 https://doi.org/10.1016/j.memsci.2024.123055.
[47] A. Katchalsky, P.F. Curran, Nonequilibrium Thermodynamics in Biophysics, Harvard University Press1965.
[48] S. Nunes, B. Wolf, On the cooccurrence of demixing and thermoreversible gelation of polymer solutions. 3. Overall view, Macromolecules 20 (8) (1987) 1952–1957.
[49] B. Alhazmi, G. Ignacz, M. Di Vincenzo, M.N. Hedhili, G. Szekely, S.P. Nunes, Ultraselective macrocycle membranes for pharmaceutical ingredients separation in organic solvents, Nat. Commun. 15 (1) (2024) 7151, https://doi.org/10.1038/s41467-024-51548-7.
[50] G. Ignacz, A.K. Beke, G. Szekely, Data-driven investigation of process solvent and membrane material on organic solvent nanofiltration, J. Membr. Sci. 674 (2023) 121519, https://doi.org/10.1016/j.memsci.2023.121519.
[51] A.K. Beke, G. Ignacz, G. Szekely, Universal solution to the membrane selectivity challenge: separation merit and efficiency, Adv. Membr (2024) 100103, https://doi.org/10.1016/j.advmem.2024.100103.
[52] P. Aimar, M. Meireles, V. Sanchez, A contribution to the translation of retention curves into pore size distributions for sieving membranes, J. Membr. Sci. 54 (3) (1990) 321–338, https://doi.org/10.1016/S0376-7388(00)80618-3.
[53] S. Singh, K.C. Khulbe, T. Matsuura, P. Ramamurthy, Membrane characterization by solute transport and atomic force microscopy, J. Membr. Sci. 142 (1) (1998) 111–127, https://doi.org/10.1016/S0376-7388(97)00329-3.
[54] D. Kim, N.L. Le, S.P. Nunes, The effects of a co-solvent on fabrication of cellulose acetate membranes from solutions in 1-ethyl-3-methylimidazolium acetate, J. Membr. Sci. 520 (2016) 540–549, https://doi.org/10.1016/j.memsci.2016.08.015.
[55] C.M. Hansen, Hansen Solubility Parameters: a User's Handbook, CRC press2007.
[56] S. Kim, J. Chen, T. Cheng, A. Gindulyte, J. He, S. He, Q. Li, B.A. Shoemaker, P. A. Thiessen, B. Yu, L. Zaslavsky, J. Zhang, E.E. Bolton, PubChem 2023 update, Nucleic Acids Res. 51 (D1) (2022) D1373–D1380, https://doi.org/10.1093/nar/gkac956.
[57] L. Wang, T. Cao, J.E. Dykstra, S. Porada, P.M. Biesheuvel, M. Elimelech, Salt and water transport in reverse osmosis membranes: beyond the solution-diffusion model, Environ. Sci. Technol. 55 (24) (2021) 16665–16675, https://doi.org/10.1021/acs.est.1c05649.
[58] P.M. Biesheuvel, S. Porada, M. Elimelech, J.E. Dykstra, Tutorial review of reverse osmosis and electrodialysis, J. Membr. Sci. 647 (2022) 120221, https://doi.org/10.1016/j.memsci.2021.120221.
[59] Y. Sun, S. Zhou, G. Qin, J. Guo, Q. Zhang, S. Li, S. Zhang, A chemical-induced crystallization strategy to fabricate poly(ether ether ketone) asymmetric membranes for organic solvent nanofiltration, J. Membr. Sci. 620 (2021) 118899, https://doi.org/10.1016/j.memsci.2020.118899.
[60] K. Hendrix, M. Vaneynde, G. Koeckelberghs, I.F.J. Vankelecom, Synthesis of modified poly(ether ether ketone) polymer for the preparation of ultrafiltration and nanofiltration membranes via phase inversion, J. Membr. Sci. 447 (2013) 96–106, https://doi.org/10.1016/j.memsci.2013.07.006.
[61] K. Hendrix, S. Vandoorne, G. Koeckelberghs, I.F.J. Vankelecom, SRNF membranes for edible oil purification: introducing free amines in crosslinked PEEK to increase membrane hydrophilicity, Polymer 55 (6) (2014) 1307–1316, https://doi.org/10.1016/j.polymer.2013.11.039.
[62] X. Li, S. De Feyter, I.F.J. Vankelecom, Poly(sulfone)/sulfonated poly(ether ether ketone) blend membranes: morphology study and application in the filtration of alcohol based feeds, J. Membr. Sci. 324 (1) (2008) 67–75, https://doi.org/10.1016/j.memsci.2008.06.055.
[63] N. Alqadhi, D.G. Oldal, K. Gopalsamy, M.A. Abdulhamid, G. Szekely, Poly(ether-ether-ketone) copolymers featuring sulfonyl moieties for organic solvent nanofiltration membranes, Separ. Purif. Technol. 355 (2025) 129628, https://doi.org/10.1016/j.seppur.2024.129628.
[64] M.A. Abdulhamid, R. Hardian, G. Szekely, Waltzing around the stereochemistry of membrane crosslinkers for precise molecular sieving in organic solvents, J. Membr. Sci. 638 (2021) 119724, https://doi.org/10.1016/j.memsci.2021.119724.
[65] K. Hendrix, M. Van Eynde, G. Koeckelberghs, I.F.J. Vankelecom, Crosslinking of modified poly(ether ether ketone) membranes for use in solvent resistant nanofiltration, J. Membr. Sci. 447 (2013) 212–221, https://doi.org/10.1016/j.memsci.2013.07.002.
[66] M.G. Buonomenna, G. Golemme, J.C. Jansen, S.H. Choi, Asymmetric PEEKWC membranes for treatment of organic solvent solutions, J. Membr. Sci. 368 (1) (2011) 144–149, https://doi.org/10.1016/j.memsci.2010.11.036.
[67] Y. Sun, T. Sun, J. Pang, N. Cao, C. Yue, J. Wang, X. Han, Z. Jiang, Poly(aryl ether ketone) membrane with controllable degree of sulfonation for organic solvent nanofiltration, Separ. Purif. Technol. 273 (2021) 118956, https://doi.org/10.1016/j.seppur.2021.118956.
[68] M.F. Jimenez Solomon, Y. Bhole, A.G. Livingston, High flux membranes for organic solvent nanofiltration (OSN)—Interfacial polymerization with solvent activation, J. Membr. Sci. 423–424 (2012) 371–382, https://doi.org/10.1016/j.memsci.2012.08.030.
[69] Y.H. See Toh, F.W. Lim, A.G. Livingston, Polymeric membranes for nanofiltration in polar aprotic solvents, J. Membr. Sci. 301 (1) (2007) 3–10, https://doi.org/10.1016/j.memsci.2007.06.034.
[70] S. Yuan, J. Wang, X. Li, J. Zhu, A. Volodine, X. Wang, J. Yang, P. Van Puyvelde, B. Van der Bruggen, New promising polymer for organic solvent nanofiltration: oxidized poly (arylene sulfide sulfone), J. Membr. Sci. 549 (2018) 438–445, https://doi.org/10.1016/j.memsci.2017.12.036.
[71] M.H. Abdellah, L. Pérez-Manríquez, T. Puspasari, C.A. Scholes, S.E. Kentish, K.-V. Peinemann, A catechin/cellulose composite membrane for organic solvent nanofiltration, J. Membr. Sci. 567 (2018) 139–145, https://doi.org/10.1016/j.memsci.2018.09.042.
[72] L. Pérez-Manríquez, A.R. Behzad, K.-V. Peinemann, Sub-6 nm thin cross-linked dopamine films with high pressure stability for organic solvent nanofiltration, Macromol. Mater. Eng. 301 (12) (2016) 1437–1442, https://doi.org/10.1002/mame.201600107.
[73] S. Ilyas, N. Joseph, A. Szymczyk, A. Volodin, K. Nijmeijer, W.M. de Vos, I.F. J. Vankelecom, Weak polyelectrolyte multilayers as tunable membranes for solvent resistant nanofiltration, J. Membr. Sci. 514 (2016) 322–331, https://doi.org/10.1016/j.memsci.2016.04.073.
[74] M. Mertens, C. Van Goethem, M. Thijs, G. Koeckelberghs, I.F.J. Vankelecom, Crosslinked PVDF-membranes for solvent resistant nanofiltration, J. Membr. Sci. 566 (2018) 223–230, https://doi.org/10.1016/j.memsci.2018.08.051.
[75] S. Behnke, M. Ulbricht, Thin-film composite membranes for organophilic nanofiltration based on photo-cross-linkable polyimide, React. Funct. Polym. 86 (2015) 233–242, https://doi.org/10.1016/j.reactfunctpolym.2014.09.027.
[76] D. Chen, C. Yan, X. Li, L. Liu, D. Wu, X. Li, A highly stable PBI solvent resistant nanofiltration membrane prepared via versatile and simple crosslinking process, Separ. Purif. Technol. 224 (2019) 15–22, https://doi.org/10.1016/j.seppur.2019.04.077.
[77] Y. Xu, F. You, H. Sun, L. Shao, Realizing mussel-inspired polydopamine selective layer with strong solvent resistance in nanofiltration toward sustainable reclamation, ACS Sustain. Chem. Eng. 5 (6) (2017) 5520–5528, https://doi.org/10.1021/acssuschemeng.7b00871.
[78] X. Li, P. Vandezande, I.F.J. Vankelecom, Polypyrrole modified solvent resistant nanofiltration membranes, J. Membr. Sci. 320 (1) (2008) 143–150, https://doi.org/10.1016/j.memsci.2008.03.061.

[79] Y. Li, J. Xue, X. Zhang, B. Cao, P. Li, Formation of macrovoid-free PMDA-MDA polyimide membranes using a Gelation/Non-Solvent-Induced phase separation method for organic solvent nanofiltration, Ind. Eng. Chem. Res. 58 (16) (2019) 6712–6720, https://doi.org/10.1021/acs.iecr.9b00623.
[80] I.B. Valtcheva, S.C. Kumbharkar, J.F. Kim, Y. Bhole, A.G. Livingston, Beyond polyimide: crosslinked polybenzimidazole membranes for organic solvent nanofiltration (OSN) in harsh environments, J. Membr. Sci. 457 (2014) 62–72, https://doi.org/10.1016/j.memsci.2013.12.069.
[81] H.-Y. Jang, J.R. Johnson, Y. Ma, R. Mathias, D.A. Bhandari, R.P. Lively, Torlon® hollow fiber membranes for organic solvent reverse osmosis separation of complex aromatic hydrocarbon mixtures, AIChE J. 65 (12) (2019) e16757, https://doi.org/10.1002/aic.16757.
[82] B. Li, S. Japip, J.-Y. Lai, T.-S. Chung, Revitalize integrally skinned hollow fiber membranes with spatially impregnated 3D-macrocycles for organic solvent nanofiltration, Chem. Eng. J. 422 (2021) 130015, https://doi.org/10.1016/j.cej.2021.130015.
[83] A. Asadi Tashvigh, T.-S. Chung, Robust polybenzimidazole (PBI) hollow fiber membranes for organic solvent nanofiltration, J. Membr. Sci. 572 (2019) 580–587, https://doi.org/10.1016/j.memsci.2018.11.048.
[84] J. Su, X. Lv, S. Li, Y. Jiang, S. Liu, X. Zhang, H. Li, B. Su, High separation performance thin film composite and thin film nanocomposite hollow fiber membranes via interfacial polymerization for organic solvent nanofiltration, Separ. Purif. Technol. 278 (2021) 119567, https://doi.org/10.1016/j.seppur.2021.119567.
[85] H. Abadikhah, E.N. Kalali, S. Behzadi, S.A. Khan, X. Xu, M.E. Shabestari, S. Agathopoulos, High flux thin film nanocomposite membrane incorporated with functionalized TiO2@reduced graphene oxide nanohybrids for organic solvent nanofiltration, Chem. Eng. Sci. 204 (2019) 99–109, https://doi.org/10.1016/j.ces.2019.04.022.
[86] S. Darvishmanesh, F. Tasselli, J.C. Jansen, E. Tocci, F. Bazzarelli, P. Bernardo, P. Luis, J. Degrève, E. Drioli, B. Van der Bruggen, Preparation of solvent stable polyphenylsulfone hollow fiber nanofiltration membranes, J. Membr. Sci. 384 (1) (2011) 89–96, https://doi.org/10.1016/j.memsci.2011.09.003.
[87] S.-P. Sun, S.-Y. Chan, T.-S. Chung, A slow–fast phase separation (SFPS) process to fabricate dual-layer hollow fiber substrates for thin-film composite (TFC) organic solvent nanofiltration (OSN) membranes, Chem. Eng. Sci. 129 (2015) 232–242, https://doi.org/10.1016/j.ces.2015.02.043.
[88] Hui M. Tham, K.Y. Wang, D. Hua, S. Japip, T.-S. Chung, From ultrafiltration to nanofiltration: Hydrazine cross-linked polyacrylonitrile hollow fiber membranes for organic solvent nanofiltration, J. Membr. Sci. 542 (2017) 289–299, https://doi.org/10.1016/j.memsci.2017.08.024.
[89] D.Y. Xing, S.Y. Chan, T.-S. Chung, The ionic liquid [EMIM]OAc as a solvent to fabricate stable polybenzimidazole membranes for organic solvent nanofiltration, Green Chem. 16 (3) (2014) 1383–1392, https://doi.org/10.1039/C3GC41634H.
[90] M.H. Davood Abadi Farahani, T.-S. Chung, Solvent resistant hollow fiber membranes comprising P84 polyimide and amine-functionalized carbon nanotubes with potential applications in pharmaceutical, food, and petrochemical industries, Chem. Eng. J. 345 (2018) 174–185, https://doi.org/10.1016/j.cej.2018.03.153.
[91] B. Zhao, G.M. Shi, K.Y. Wang, J.-Y. Lai, T.-S. Chung, Employing a green cross-linking method to fabricate polybenzimidazole (PBI) hollow fiber membranes for organic solvent nanofiltration (OSN), Separ. Purif. Technol. 255 (2021) 117702, https://doi.org/10.1016/j.seppur.2020.117702.
[92] G. Falca, V.-E. Musteata, A.R. Behzad, S. Chisca, S.P. Nunes, Cellulose hollow fibers for organic resistant nanofiltration, J. Membr. Sci. 586 (2019) 151–161, https://doi.org/10.1016/j.memsci.2019.05.009.
[93] H.M. Tham, T.-S. Chung, One-step cross-linking and tannic acid modification of polyacrylonitrile hollow fibers for organic solvent nanofiltration, J. Membr. Sci. 610 (2020) 118294, https://doi.org/10.1016/j.memsci.2020.118294.
[94] S. Jeon, A. Nishitani, L. Cheng, L.-F. Fang, N. Kato, T. Shintani, H. Matsuyama, One-step fabrication of polyamide 6 hollow fibre membrane using non-toxic diluents for organic solvent nanofiltration, RSC Adv. 8 (35) (2018) 19879–19882, https://doi.org/10.1039/C8RA03328E.
[95] S.M. Dutczak, C.R. Tanardi, K.K. Kopeć, M. Wessling, D. Stamatialis, "Chemistry in a spinneret" to fabricate hollow fibers for organic solvent filtration, Separ. Purif. Technol. 86 (2012) 183–189, https://doi.org/10.1016/j.seppur.2011.11.003.
[96] Y. Dai, M.D. Guiver, G.P. Robertson, Y.S. Kang, Effect of Hexafluoro-2-propanol substituents in polymers on gas permeability and fractional free volume, Macromolecules 38 (23) (2005) 9670–9678, https://doi.org/10.1021/ma051662h.

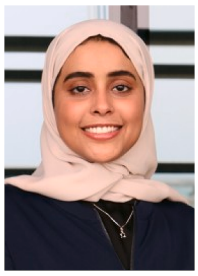

Banan Alhazmi received her MSc and recently defended her PhD in Environmental Science and Engineering at KAUST on new materials for highly selective membranes and fractionation of complex mixtures of pharmaceutical ingredients in organic solvents. She is currently environmental consultant at the Golden Ratio Institute. Her research interests are on sustainability, membrane technology and science-policy interface.



Lakshmeesha Upadhyaya received his MSc and PhD (Erasmus Mundus) in Physical Chemistry of Materials, Membrane Engineering from the University of Montpellier, France. He was postdoctoral researcher at the University of Arkansas and was research scientist at KAUST, working on hollow fiber development and applications such as air dehumidification.



Shanshan Hong received her MSc degree in Environmental Science and Engineering from KAUST and is currently PhD student in Chemistry also at KAUST. Her research focuses on developing new reactions and materials for interfacial polymerization applied to membranes.



Gergo Ignacz received his BS degree in Chemical Engineering from the Budapest University of Technology and Economics, and MRes degree in Chemical Engineering from the University of Manchester. Gergo was a PhD student and now a postdoctoral researcher at KAUST. His research focuses on developing machine learning networks in the domain of material and membrane science.



Radoslaw Gorecki received his MSc and PhD in Sustainable Energy and Industrial PhD in Chemical Engineering and Biophysics from the Technical University of Denmark, having worked also as industrial researcher at Aquaporin A/S. He is now research scientist at KAUST. His research focuses is on advanced methods of x-ray synchrotron imaging and electron microscopy applied to membranes, as well as block copolymer membranes.



Maik Tepper received his MSc and Dr. Ing in Chemical Process Engineering from RWTH Aachen University working on the development of hollow fibers and spinneret designs. He is now research and development team lead for membrane technology at Vantive in Germany.



Hannah Rothau is Professor of Technical and Macromolecular Chemistry for Water Research at the University of Duisburg-Essen, Germany. She received her Dr.-Ing from the RWTH Aachen University, Germany. Her research focus is on membrane development.



Matthias Wessling is Alexander von Humboldt Professor of Chemical Product and Process Design and Vice Rector Transfer at RWTH Aachen, Germany. He is member of the scientific directorate of DWI Leibniz Institute for Interactive Materials in Germany. He received his PhD in Chemical Engineering from the University of Twente, Netherlands. He is elected member of the German Academy of Science (Leopoldina). His research interests are sustainable membrane processes and fundaments of mass transport through synthetic membranes.



Gyorgy Szekely received his MSc in Chemical Engineering from the Technical University of Budapest, and PhD in Chemistry from the Technical University of Dortmund. He worked in the pharmaceutical R&D Center of Hovione, and as an IAESTE Fellow at the University of Tokyo. He has held positions at Imperial College London and The University of Manchester. He received the Distinguished Visiting Fellowship of the Royal Academy of Engineering. He is an Associate Professor at KAUST. He focuses on sustainable separations through a combination of materials science and process engineering.



Suzana Nunes is Professor of Chemical and Environmental Science and Engineering at KAUST. She has a Doctor of Science in Chemistry from the University of Campinas, Brazil, and was a Humboldt Postdoctoral Fellow at the Johannes Gutenberg University, Mainz University, Germany. She is fellow of TWAS, RSC, NAMS, ACIESP, honorary EMS member and international Loreal-UNESCO laureate. Her research focus is on new polymeric materials for membranes.